Electronic structure and physical properties of the spinel-type phase of BeP_2N_4 from all-electron density functional calculations

W. Y. Ching,[1] Sitram Aryal,[1] Paul Rulis,[1] and Wolfgang Schnick[2]

[1]*Department of Physics, University of Missouri–Kansas City, Kansas City, Missouri 64110, USA*
[2]*Department of Chemistry, University of Munich (LMU), D-81377 Munich, Germany*
(Received 7 December 2010; revised manuscript received 19 February 2011; published 11 April 2011)

Using density-functional-theory-based *ab initio* methods, the electronic structure and physical properties of the newly synthesized nitride BeP_2N_4 with a phenakite-type structure and the predicted high-pressure spinel phase of BeP_2N_4 are studied in detail. It is shown that both polymorphs are wide band-gap semiconductors with relatively small electron effective masses at the conduction-band minima. The spinel-type phase is more covalently bonded due to the increased number of P-N bonds for P at the octahedral sites. Calculations of mechanical properties indicate that the spinel-type polymorph is a promising superhard material with notably large bulk, shear, and Young's moduli. Also calculated are the Be K, P K, P L_3, and N K edges of the electron energy-loss near-edge structure for both phases. They show marked differences because of the different local environments of the atoms in the two crystalline polymorphs. These differences will be very useful for the experimental identification of the products of high-pressure syntheses targeting the predicted spinel-type phase of BeP_2N_4.

I. INTRODUCTION

Recently, the new beryllium phosphorus nitride BeP_2N_4 has been synthesized at high temperature (1500 °C) and high pressure (5 GPa) using the multianvil method. According to the crystal structure determination, BeP_2N_4 adopts the phenakite-type of structure, and thus, it is isostructural with Be_2SiO_4 and β-Si_3N_4.[1] Unlike the isoelectronic ternary nitrides of the heavier alkaline-earth elements MP_2N_4, with M = Ca, Sr, or Ba,[2–4] BeP_2N_4 has to be classified as a true double nitride and not as a beryllium nitridophosphate because both Be and P retain coordination number 4 in analogy with the respective binary nitrides α-Be_3N_2 [5] and α-P_3N_5.[6,7]

More than 10 years ago, the high-pressure synthesis and characterization of cubic spinel-type Si_3N_4 (denoted as $\gamma-Si_3N_4$ or c-Si_3N_4) was seen as a revolutionary discovery because it was the first experimental evidence for a high-pressure phase of this very important nonoxide ceramic material. Ceramics made up of Si_3N_4 cover a broad range of applications. Predominant materials properties of this compound are chemical inertness, low density, high hardness, and mechanical strength.[8,9] As expected, the high-pressure spinel-type material γ-Si_3N_4 turned out to be a very hard material.[10] From a structural point of view, spinel-type Si_3N_4 attracted specific attention as it was one of the first compounds containing Si atoms, which are octahedrally coordinated by N.[11] These findings have stimulated many experimental and theoretical investigations on γ-Si_3N_4.[12,13] As a consequence, the discovery of spinel-type $\gamma-Si_3N_4$ has evoked a search for other isoelectronic and isostructural compounds with comparable materials properties. In this context, Ga_3O_3N,[14] c-Ge_3N_4,[15] and the hypothetical c-Fe_3N_4 [16] have been described in the literature. Another promising isoelectronic compound is BeP_2N_4, which, under high pressure, might form a spinel-type phase with interesting properties as well.[1] Furthermore, spinel-type BeP_2N_4 would contain an unprecedented coordination geometry for phosphorus atoms, namely, PN_6 octahedra, which have only been predicted in the hypothetical δ-P_3N_5.[17] Accordingly, it would be extremely

exciting if the spinel-type phase of BeP_2N_4 with P at the octahedral site could be synthesized and its physical properties could be explored. Recently, density-functional-theory-based *ab initio* calculations have supported the possible existence of a spinel-type phase of BeP_2N_4 at pressures around 24 GPa, which are attainable by state-of-the-art high-pressure experimental techniques.[1] High-pressure polymorphs of related polymeric and covalent nitrides [e.g., γ-Si_3N_4 [12,13] or γ-P_3N_5,[18]] which were typically synthesized at higher temperatures, turned out to be quenchable. The relative stability of different structure candidates of BeP_2N_4 under pressure has been evaluated, and the hypothetical spinel-type polymorph of BeP_2N_4 turned out to be stable under high pressure. Due to its covalent character, this high-pressure polymorph should be quenchable as a metastable phase at ambient conditions as well. Structural optimization of the latter phase has been reported.[1] However, no further electronic, spectroscopic, or elastic properties of hypothetical spinel-type BeP_2N_4 have been calculated so far.

In this contribution, a thorough theoretical evaluation of the physical properties anticipated for spinel-type BeP_2N_4 will be given. The calculation of the physical properties for BeP_2N_4 is based on the experimentally determined structure for the phenakite-type phase and the density functional theory (DFT) predicted structure for the spinel-type phase.[1] Because the experimentally determined structure for the phenakite-type phase using Rietveld refinement on powdered samples may be less accurate, the theoretically refined structure for the phenakite-type BeP_2N_4 is also used for the electronic structure and bonding calculations.[1]

The crystal structures for these two structures are sketched in Fig. 1, and their lattice parameters summarized in Table I. The phenakite-type structure has a rhombohedral unit cell with lattice parameters of a = 7.8369 Å, α = 108.12° (space group R-3, No. 148, Z = 6) with 42 atoms in the primitive cell. There are two crystallographically nonequivalent P sites (P1 and P2), which are tetrahedrally coordinated by four nonequivalent N (N1, N2, N3, and N4). The structure can be considered as consisting of corner-sharing BeN_4 and PN_4
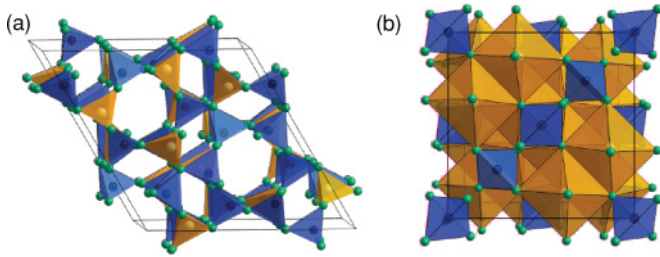
FIG. 1. (Color online) Polyhedral models of BeP_2N_4: (a) phenakite type and (b) spinel type. BeN_4 tetrahedra, dark gray (blue); PN_4 tetrahedra and octahedra, light gray (orange).

tetrahedra. The predicted spinel-type structure has a face-centered cubic structure with 14 atoms in the primitive unit cell and lattice parameters of $a = 7.4654$ Å (space group Fd-$3m$, No. 227, $Z = 2$). The positions for Be, P, and N are each uniquely defined, with Be and P occupying the tetrahedral and octahedral sites of the spinel structure type, respectively. This is a theoretically optimized structure by DFT calculations using the generalized gradient approximation with projector-augmented wave potential (PAW-GGA) and the Vienna Ab-Initio Simulation Package (VASP).[19–21] The inverse spinel structure for BeP_2N_4 was also investigated but was found to have a higher total energy than the normal spinel. The predicted normal spinel structure of BeP_2N_4 was adopted for the electronic structure and physical properties calculations.

In this paper, we report the results of detailed calculations of a wide spectrum of physical properties of both the phenakite- and spinel-type phases of BeP_2N_4, including the electronic structure and bonding, valence-band optical properties, core-level excitations, and the mechanical properties. We believe that a careful, detailed comparison of the properties of the two phases will yield additional insights and will facilitate the eventual identification of the anticipated spinel-type phase of BeP_2N_4. In Sec. II, we briefly discuss the methods used in these calculations. The calculated results are presented and discussed in Sec. III. A brief summary is presented in Sec. IV.

II. METHODS OF CALCULATION

The main method used for the electronic structure and property calculations of BeP_2N_4 is the orthogonalized linear combination of atomic orbitals (OLCAO) method.[22] This is an all-electron method based on the local density approximation (LDA) of density functional theory. In the OLCAO method, the atomic orbitals (expanded in terms of the Gaussian type of orbitals) are used in the basis expansion of the Bloch function. In the present calculation, a full basis set (FB) consisting of the $1s$, $2s$, $3s$, $2p$, and $3p$ atomic orbitals of Be and N and the $1s$, $2s$, $3s$, $4s$, $2p$, $3p$, $4p$, and $3d$ orbitals for P was used. For optical and spectral calculations, an extra shell of atomic orbitals for each element is added to the FB set to improve the accuracy of the higher unoccupied conduction-band (CB) states. This is referred to as an extended basis. The OLCAO method is extremely efficient and versatile for electronic structure and properties calculations especially for large complex systems due to the flexible choice of the basis set and the ability to efficiently evaluate all multicenter interaction integrals. The method has been successfully employed in the investigations

TABLE I. Comparison of phenakite- and spinel-type phases of BeP_2N_4.

Crystal	Phenakite type	Exp. phenakite type	Theory spinel type
a (Å), α	7.8369 (108.12°)	7.8925 (108.15°)	7.4654 (90°)
Z	6	6	2
Space group	R-3 (No. 148)	R-3 (No. 148)	Fd-$3m$ (No. 227)
Cell volume/FU (Å³)	64.668	65.988	54.113
Band gap	3.31 (direct)	3.97 (direct)	3.60 (indirect)
m_e^*	0.56	0.69	0.60
Q^* (electrons)			
Be	1.25	1.28	1.40
P	3.38, 3.34	3.30, 3.29	3.51
N	6.00, 5.99, 6.05, 5.99	6.02, 6.02, 6.04, 6.03	5.90
BO (electron) and BL (Å) (in parentheses)			
Be-N	0.346 (1.481)	0.275 (1.746)	0.313 (1.762) (4)
	0.238 (1.703)	0.281 (1.732)	
	0.262 (1.754)	0.271 (1.726)	
	0.265 (1.810)	0.271 (1.760)	
P1-N	0.387 (1.619)	0.372 (1.654)	0.236 (1.822) (6)
	0.404 (1.639)	0.377 (1.651)	
	0.345 (1.719)	0.380 (1.645)	
	0.329 (1.729)	0.385 (1.643)	
P2-N	0.384 (1.603)	0.378 (1.655)	
	0.385 (1.617)	0.381 (1.648)	
	0.360 (1.692)	0.369 (1.645)	
	0.368 (1.714)	0.391 (1.636)	
Total BO/FU	4.076	4.131	4.084
Reference index	2.24	2.18	2.30

of many complex inorganic[23–27] and organic materials,[28] noncrystalline compounds,[29] biomolecules,[30] grain boundaries, surfaces, and interfaces.[31–34] This method bears many similarities to both CRYSTAL[35] and DMOL.[36]

One of the most useful features in the OLCAO method is the calculation of the Mulliken effective charge Q_α^* on each atom and the bond order (BO) value $\rho_{\alpha\beta}$ between each pair of atoms defined by

$$Q_\alpha^* = \sum_i \sum_{n,occ} \sum_{j,\beta} C_{i\alpha}^{*n} C_{j\beta}^n S_{i\alpha,j\beta}, \qquad (1)$$

$$\rho_{\alpha\beta} = \sum_{n,occ} \sum_{i,j} C_{i\alpha}^{*n} C_{j\beta}^n S_{i\alpha,j\beta}. \qquad (2)$$

Calculation of Q^* and BO enables us to estimate the charge transfer among the atoms and the relative bond strength of a particular bond. In Eqs. (1) and (2), i and j label the orbital quantum numbers, and n is the band index. $S_{i\alpha,j\beta}$ is the overlap matrix between the OLCAO Bloch sums, and $C_{j\beta}^n$ is the eigenvector coefficients of the wave function. Because the Mulliken scheme[37] works best when the basis functions are localized, a minimal basis set, which has one less shell of orbitals than the FB set, is used for effective charge and bond order calculations.

Another important application of the OLCAO method is the calculation of the optical dielectric function according to the following expression for crystalline solids using the *ab initio* wave functions obtained from the OLCAO calculation:

$$\varepsilon_2(\hbar\omega) = \frac{e^2}{\pi m \omega^2} \int_{BZ} dk^3 \sum_{n,l} |\langle \psi_n(\mathbf{k},\mathbf{r})| - i\hbar\nabla |\psi_l(\mathbf{k},\mathbf{r})\rangle|^2$$
$$\times \delta[E_n(\mathbf{k}) - E_l(\mathbf{k}) - \hbar\omega]. \qquad (3)$$

Here $\hbar\omega$ is the transition energy, and the summation is over all occupied states ℓ and unoccupied states n. The integration over the Brillouin zone (BZ) is carried out with a large number of $\mathbf{k}$ points, and an extended basis was used. There are other more elaborate methods for excited state calculations in crystals involving many-body theory or time-dependent density functional theory.[38] They are so far limited to crystals of relatively simple structures.

Electron energy-loss near-edge structure (ELNES) spectroscopy and x-ray absorption near-edge structure (XANES) spectroscopy are important experimental characterization techniques.[39] The ELNES-XANES Be K, N K, P K, and P L_3 edges of the BeP$_2$N$_4$ polymorphs were calculated using the supercell-OLCAO method.[40,41] This method takes into account the core-hole effect, and it has been successfully applied to many crystalline materials within the last 10 years, resulting in good to excellent agreement with experimentally determined edges.[31,42–51] Here we briefly capture the essential steps in the calculation. The initial state of each edge calculation is the ground state of a supercell that contains the target atom (e.g., Be). The final states, calculated separately, are the conduction-band states with the excited electron from the core (e.g., $1s$ of Be) placed at the bottom of the CB. It should be pointed out that in the final-state calculation, the system remains charge neutral by including the electron in the otherwise empty CB during charge density accumulation for construction of the self-consistent potential. The interaction between the excited electron in the CB and the hole in the core is accounted for in the self-consistent iterations of the final-state calculation. The presence of the core hole can significantly modify the final-state wave function and hence the ELNES spectrum. The final ELNES features are obtained by evaluating the transition strength in the dipole approximation and including the dipole matrix elements between the initial state ($1s$ for the K edge and $2p$ for the L edge) and the final states (core-hole states). The explicit inclusion of the dipole matrix elements calculated from the *ab initio* wave functions automatically ensures that the selection rules are fully satisfied. All calculated final spectra are broadened by a Gaussian with a full width at half maximum of 1.0 eV for consistency. For easy comparison, all spectra for the same edge are normalized to unit area. The energy scale of the spectra is determined by the difference of the total energies of the ground-state and the final-state supercell calculations. In the present study, we used $2 \times 2 \times 2$ supercells for both the phenakite- and the spinel-type phases that contained 336 atoms and 112 atoms, respectively. These supercells are sufficiently large to ensure that spurious interactions with the core holes in adjacent replicated supercells are negligible.[40,41]
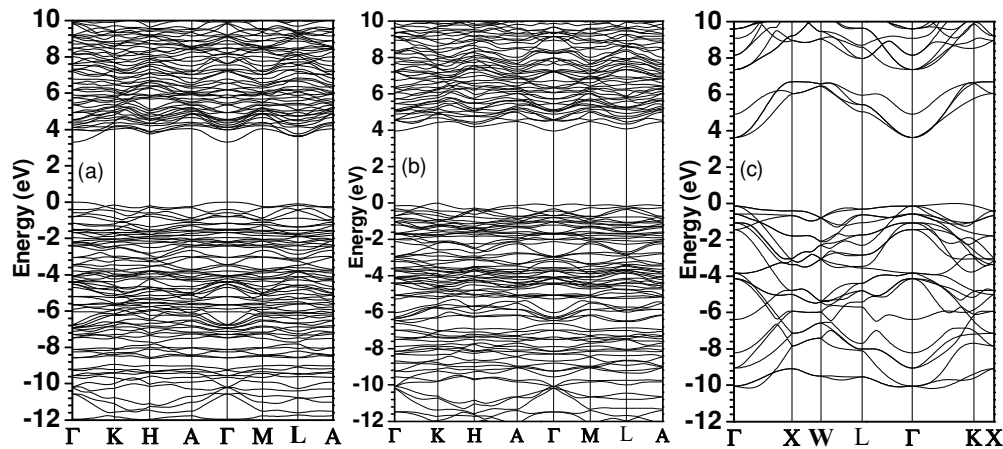

FIG. 2. Band structures of BeP$_2$N$_4$: (a) phenakite type using experimental structure, (b) phenakite type using theoretically refined structure, and (c) spinel type.

For the mechanical and elastic properties calculations, we used VASP together with some in-house-developed scripts. In the present study for BeP_2N_4, small strains of -1% (compression) and $+1\%$ (stretching) were applied to the equilibrium structure in each independent strain element of the crystal.[52] The deformed structure was then fully optimized while keeping the cell volume constant. Six components of the stress data σ_i (xx, yy, zz, yz, zx, and xy) under applied strains ε_i were used to solve the system of linear equations for the elastic tensor C_{ij}. The mechanical properties in the form of bulk modulus K, shear modulus G, Young's modulus E, and Poisson's ratio η were obtained from C_{ij} using the Voigt-Reuss-Hill approximation.[53] This approach has been used to study the mechanical properties of many ceramic materials,[54] $\gamma-Al_2O_3$,[55] bioceramic hydroxyapatite,[34] α and β phases of tricalcium phosphates,[27] and an intergranular glassy film model between prismatic faces of β-Si_3N_4.[34]

III. RESULTS

A. Electronic structure and bonding

Figure 2 shows the calculated band structures of the three crystal structures of BeP_2N_4: the experimentally determined and the theoretically refined structures for phenakite-like BeP_2N_4 and the theoretically predicted spinel structure. It is noted that the theoretically refined structure for BeP_2N_4 has slightly larger lattice constants and crystal volume, which may affect its electronic structure and bonding to a certain extent. Both types of crystals are large-gap semiconductors. The phenakite-like phase with two slightly differing structures has direct band gaps of 3.31 and 3.97 eV at Γ, and the spinel structure has an indirect gap of 3.60 eV. These band-gap values are expected to be slightly underestimated due to the use of the LDA approximation. For the spinel phase, the calculated band gap is slightly larger than that of γ-Si_3N_4,[12] and the top of the valence band (VB) is at a point along the Γ-K direction close to

K, making it an indirect gap. The calculated electron effective mass ratios m/m_e from the band curvatures at the bottom of the CB are 0.56 and 0.69 for the two phenakite structures and 0.60 for the spinel structure. These values are similar to the electron effective mass of γ-Si_3N_4.[12]

The calculated total density of states (TDOS) and atom-resolved partial DOS (PDOS) for the three structures of BeP_2N_4 are shown in Fig. 3. There are noticeable differences between the experimentally determined structure and the theoretically refined structure for the phenakite-type phase, especially around the 10-eV range in the CB region. On the other hand, the DOS of the spinel-type phase is very different, showing a narrower upper VB and a split-off lower CB originating from the P atoms that are octahedrally coordinated by N. The large differences in the PDOS of the empty CB states between phenakite and spinel phases result in significantly different ELNES spectra, which will be discussed later. The PDOS plots also reveal that, in the phenakite-type structure, Be does not contribute to the top of the VB, whereas, in the spinel structure, Be has a significant presence at the top of the VB. Figure 3 also shows that the PDOS of P1 and P2 in the phenakite-type phase are almost identical. But there are considerable variations in the PDOS among the four N sites, especially in the results using the experimentally determined structure. In the results with the theoretically determined structure, all four N sites have a sharp N $2s$ peak at -16 eV, which is a signature of strong bonding between P and N.

The calculated Mulliken effective charges Q^*, the BO values between each pair of nearest-neighbor atoms, and their bond lengths (BLs) in the three BeP_2N_4 structures are listed in Table I. The average effective charges on the Be, P, and N ions are (1.25, 1.28), (3.36, 3.30), and (6.01, 6.03) electrons in the experimental and theoretical phenakite structures, respectively. The Q^* values for P and N in the phenakite-type structure are the averaged values over the two and four nonequivalent sites of P and N, with those
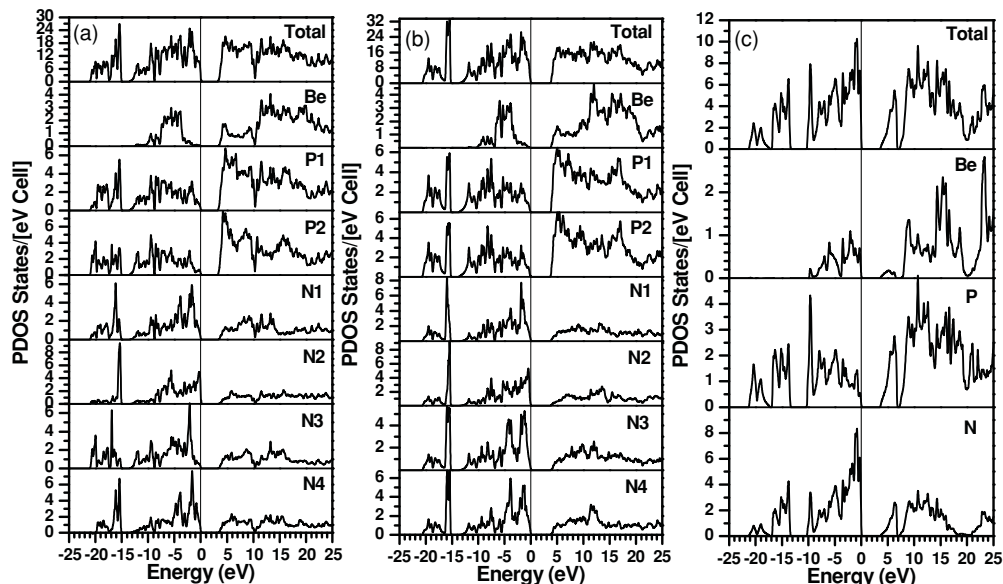

FIG. 3. Calculated DOS and PDOS of BeP_2N_4: (a) phenakite type using experimental structure, (b) phenakite type using theoretically refined structure, and (c) spinel type.

from the theoretically determined structure showing much less variation among nonequivalent sites. The effective charges for Be, P, and N in the spinel structure are 1.40, 3.51, and 5.90 electrons, respectively. This suggests that the spinel-type phase has a stronger covalent bonding character with a smaller charge transfer from Be and P to N. This is also reflected in the overall BO values. In the phenakite-type phase with the experimentally determined structure, there is a rather short (long) Be-N bond of 1.481 Å (1.810 Å) with a BO value of 0.346 (0.265). Such large variations in the Be-N bonds are absent in the theoretically refined structure. The P-N bonds in the phenakite-type phase are very strong, ranging from 0.329 to 0.404 in the experimentally determined structure and from 0.372 to 0.391 in the theoretically refined structure. Again, the latter shows much less variation among them. Although the phenakite-type phase of BeP_2N_4 forms stronger Be-N and P-N bonds mainly because of shorter BLs, the octahedrally bonded P in the spinel-type phase has more P-N bonds (6 vs 4), resulting in a comparable total crystalline BO value per formula unit (FU). The strong overall bonding in both phases is further illustrated in the calculated elastic coefficients and the mechanical properties, which will be discussed later. It should also be pointed out that the BO does not always scale with the BL. Bond angles and local atomic arrangements determine the overall bond strengths based on the calculated wave functions. Thus, the quantum mechanically determined BO value is a much more accurate indicator of the bond strength. The data on the calculated electronic structure and bonding in BeP_2N_4 are summarized in Table I.

B. Spectroscopic properties

Calculations of optical properties based on Eq. (3) and using the OLCAO method have been presented in many other published works;[23–26,28,31] therefore, a detailed description of the procedures will only be quickly summarized. Essentially, the *ab initio* wave functions at a large number of **k** points within the irreducible portion of the BZ are calculated. The dipole matrix elements of transition from all VB states to all CB states are evaluated, and the imaginary part of the dielectric function $\varepsilon_2(\hbar\omega)$ is calculated within the random phase approximation by summation over the BZ up to a high photon energy of about 30 eV. The real part of the dielectric function $\varepsilon_1(\hbar\omega)$ is obtained from $\varepsilon_2(\hbar\omega)$ by Kramers-Kronig conversion. The calculated optical dielectric functions for the two phases of BeP_2N_4 are shown in Figs. 4(a) and 4(b). For the phenakite-type phase; only the results using the experimental structure are presented. The directionally averaged optical absorption curves [$\varepsilon_2(\hbar\omega)$] for the two phases are quite different. The phenakite-type phase has a broad main absorption peak at 8.5 eV and less prominent peaks on either side of the main peak at 6.4 and 11.5 eV. The spinel-type phase has a very sharp main peak at 9.5 eV that is decorated with smaller structures. The absorption onset in the spinel-type phase is at 5.0 eV, which is larger than the indirect band gap and the direct band gap at Γ. This implies that direct transition from the VB to the CB at Γ is symmetry forbidden. The absorption in the spinel-type phase increases rather rapidly after 7.0 eV, when the transitions to the CB states above the split-off band begin. Inspection of the Cartesian components of the $\varepsilon_2(\hbar\omega)$ curves (not shown) indicates that it
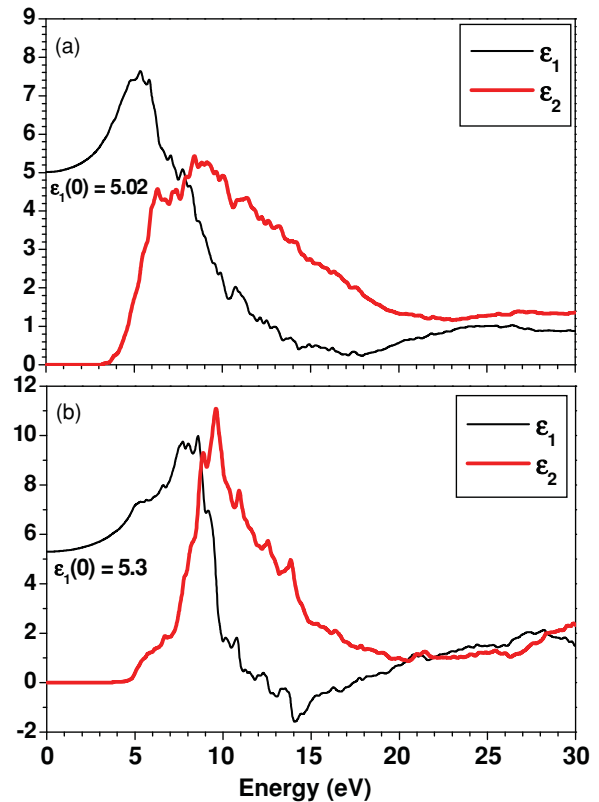

FIG. 4. (Color online) Calculated complex dielectric functions of BeP_2N_4: (a) phenakite type using experimental structure and (b) spinel type. The thick red line shows the imaginary part, and thin black line shows the real part.

is isotropic in the spinel-type phase but slightly anisotropic in the phenakite-type phase. The contribution to the main peak in the phenakite-type phase comes from the z component in the axial directional of the rhombohedral cell. The refractive index n of the two polymorphs can be estimated as the square root of $\varepsilon_1(0)$, the static optical dielectric constant. The values of n are 2.24 and 2.18 for the phenakite structures and 2.30 for the spinel-type phase.

ELNES-XANES spectroscopies are powerful characterization tools for obtaining information about the electron states of the unoccupied CB as related to the local bonding environment of a particular atom in a solid. Experimentally, the measured spectrum of a specific edge of a specific atomic species is the average spectral response over different sites of the same element that may have different local bonding configurations. For example, in γ-Si_3N_4, the measured Si K or Si L edges are the weighted combination of the spectra at the tetrahedral and the octahedral sites of the spinel-type lattice.[42] Figure 5 shows the calculated Be K, P K, P L_3, and N K edges of BeP_2N_4 in the phenakite-type (left panel) and spinel-type (right panel) phases using the supercell-OLCAO method. We do not expect to have any major differences between the experimentally determined structure and the theoretically refined structure, so only the results from the experimentally determined structure are presented. For Be K, the phenakite-type phase has a peak at 118 eV, near the edge onset, while the spinel-type phase has a very sharp peak above the edge onset at 119.3 eV. Both phases have other minor structures above the main peak.
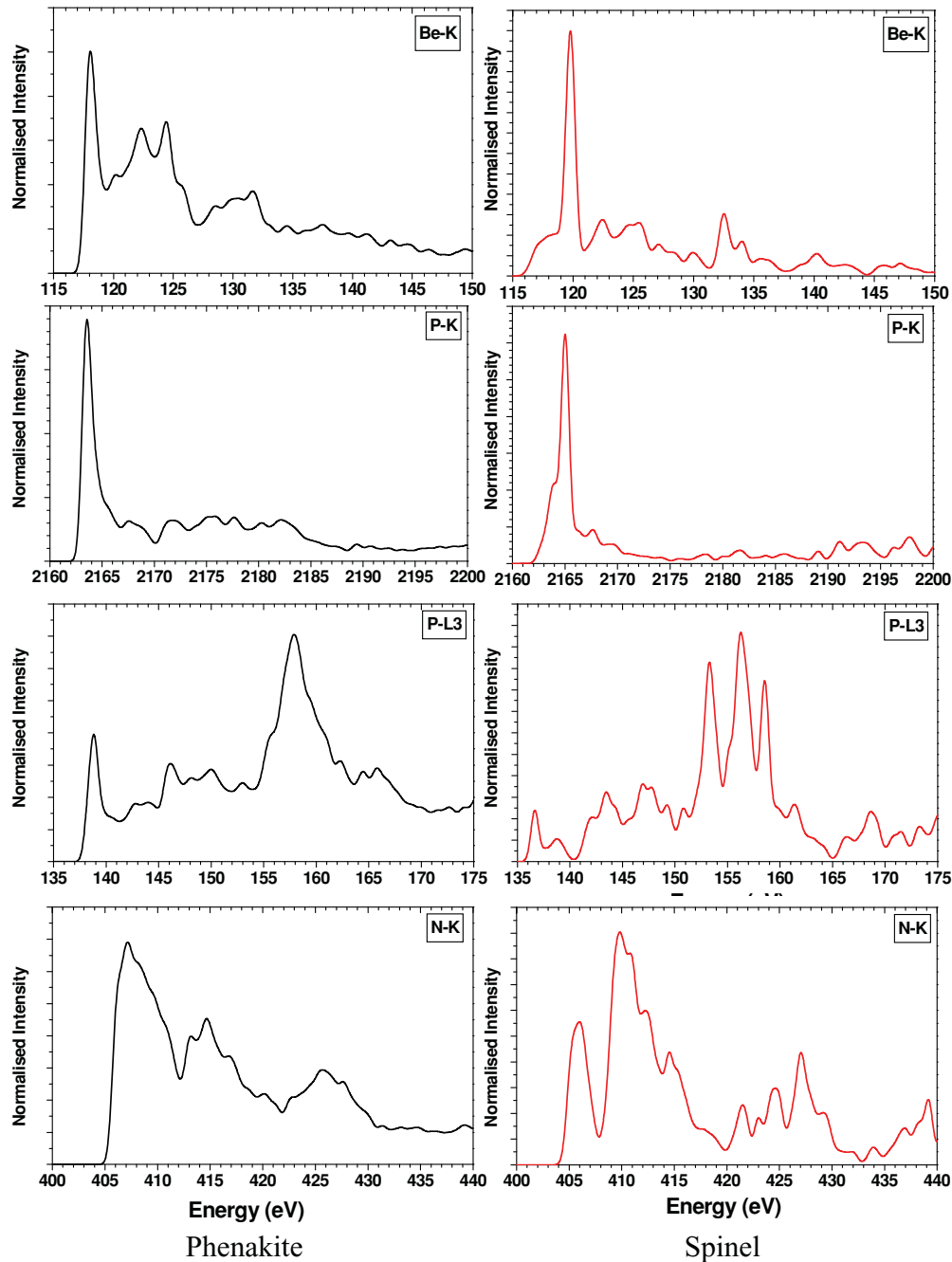
FIG. 5. (Color online) Calculated Be K, P K, P L_3, and N K edges in (left) phenakite-type and (right) spinel-type BeP_2N_4.

Such a large difference in the Be K edge could be the most distinguishable feature for phase identification. The P K edges in both phases are similar and dominated by a single sharp peak at 2163.3 and 2165.0 eV for phenakite and spinel, respectively. The latter has a shoulder-like structure on the lower energy side at 2164 eV. The L_3 edges of P, which probe the $(s + d)$-type states in the CB for transitions from the P $2p$ core, show more pronounced differences and more complicated structures. In region I, below 140 eV, the phenakite-type phase has a single peak at 138.2 eV, while the spinel polymorph has two peaks at 136.6 and 138.8 eV. In region II, above 140 eV and below 152 eV, both phases show multiple peaks. In region III, above 152 eV, the phenakite-type phase shows a single dominating

peak at 157.9 eV, whereas the spinel-type phase has three very sharp peaks at 153.2, 156.0, and 158.0 eV. Such large differences should be detectable by ELNES measurements. It should also be pointed out that the spectra for P in the phenakite-type phase are the averaged spectra of P1 and P2, which are very similar.

The comparison of the N K edges in Fig. 5 is between the single spectrum for the spinel-type phase and the averaged spectrum over four sites for the phenakite-type phase. There are considerable differences in the spectra from the four N sites. However, only the averaged spectrum will be observed experimentally. The averaged spectrum shows large differences from the single N K edge of the spinel-type phase, which
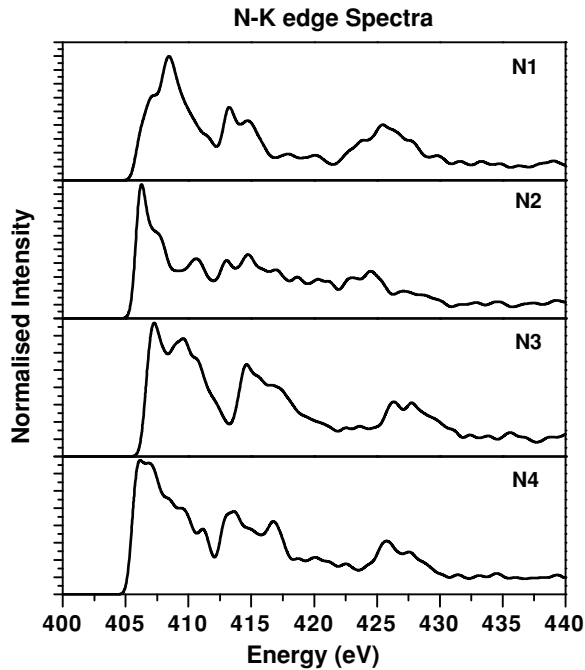
N-K edge Spectra

FIG. 6. Calculated N K edges at the four different N sites in phenakite-type BeP_2N_4.

has two prominent peaks at 405.9 and 409.9 eV that could be related to the split-off bands in the CB for the spinel-type phase. There are other additional absorption features above 420 eV for N K in the spinel-type phase. The averaged N K edge in the phenakite-type phase has three broader peaks at 407.0, 414.3, and 425.5 eV. Figure 6 shows the N K edges as calculated for the four different N sites in the phenakite-type phase, which show considerable differences. All N ions in the phenakite-type polymorph are bonded to one Be and two P. The spectral variations of the four N K edges are related to their local variations in the bond lengths and bond angles. This illustrates that the calculated spectra are very sensitive to the local environment. Presently, measurements of ELNES spectra of the phenakite-type phase of BeP_2N_4 are being prepared in order to verify our theoretical predictions. Furthermore, the calculated ELNES spectra for the predicted spinel-type phase may be used to identify, and hence prove, the formation of the high-pressure phase of BeP_2N_4.

C. Elastic and mechanical properties

The mechanical properties of the two polymorphic phases of BeP_2N_4 have been calculated using the procedures outlined

in Sec. II. The results are listed in Table II. These calculated data show that the spinel-type phase has a much larger bulk modulus, shear modulus, and Young's modulus by as much as 27%, 65%, and 56%, respectively, than the phenakite-type phase. On the other hand, the Poisson's ratio of 0.175 for the spinel-type phase is much less than that of the phenakite-type polymorph (0.238). The enhanced mechanical properties in the spinel-type phase are consistent with the increased number of bonds formed between P and N and their increasing covalent character, as discussed above. The calculated bulk moduli of 222 GPa for the phenakite-type phase and 279 GPa for the spinel-type polymorph are close to the values of 220 and 263 GPa reported in Ref. 1 using a slightly different approach and GGA potential. On the basis of these calculations, spinel-type BeP_2N_4 can be qualified as a superhard material similar to γ-Si_3N_4.

IV. CONCLUSIONS

On the basis of the preliminary theoretical calculation of a possible spinel-type high-pressure phase of BeP_2N_4,[1] we have carried out detailed *ab initio* calculations of the electronic structure, bonding characteristics, and physical properties of this newly discovered nitride. There is evidence that the structural parameters of BeP_2N_4 obtained from Rietveld refinement of the powder sample[1] are slightly different from the theoretically refined structure, which may result in slightly different electronic structures and chemical bonding. Accordingly, a careful reexamination of the crystal parameters using diffraction data from samples with a higher crystallinity or even from single crystals would be desirable. Calculations are also carried out for the predicted spinel-type phase of BeP_2N_4, whose synthesis and identification appears to be imminent. It is shown that these two phases have rather different electronic structure and spectroscopic properties. The ELNES spectra of all the edges for Be, P, and N are calculated using the supercell OLCAO method including the core-hole effect. The large difference in the Be-K edges of the two phases can be used to identify their presence and relative ratios in high-pressure reactions. Both polymorphs are wide band-gap semiconductors with relatively small electron effective masses at the CB minima. The spinel-type phase is more covalently bonded due to the increased P-N bonds for P at the octahedral sites. Calculations of mechanical properties indicate that the spinel-type polymorph of BeP_2N_4 is a promising superhard material with notably large bulk, shear, and Young's moduli. Together with its unique electronic structure and optical properties, spinel-type BeP_2N_4 may be useful for many applications once it is successfully synthesized. The present study also indicates

TABLE II. Elastic and mechanical properties of the two polymorphs of BeP_2N_4 (GPa).

	C_{11}	C_{33}	C_{44}	C_{66}	C_{12}	C_{13}	C_{14}	C_{24}	C_{56}
Phenakite	421.6	520.6	118.6	134.4	152.8	82.6	1.1	1.1	1.1
Spinel	643.2	643.2	220.7	220.7	98.0	50.2	0.0	−67.4	67.4

	Bulk Modulus	Shear Modulus	Young's Modulus	Poisson's Ratio
Phenakite	222.0	140.6	348.4	0.238
Spinel	279.3	231.6	544.4	0.175

[1] F. J. Pucher, S. R. Römer, F. W. Karau, and W. Schnick, Chem. Eur. J. **16**, 7208 (2010).

[2] F. W. Karau, L. Seyfarth, O. Oeckler, J. Senker, K. Landskron, and W. Schnick, Chem. Eur. J. **13**, 6841 (2007).

[3] F. Karau and W. Schnick, Z. Anorg. Allg. Chem. **632**, 231 (2006).

[4] F. Karau, Doctoral Thesis, Ludwig Maximilian University Munich, 2007.

[5] O. Reckeweg, C. Lind, A. Simon, and F. J. DiSalvo, Z. Naturforsch., B: J. Chem. Sci. **58**, 159 (2003).

[6] S. Horstmann, E. Irran, and W. Schnick, Angew. Chem., Int. Ed. Engl. **36**, 1873 (1997).

[7] S. Horstmann, E. Irran, and W. Schnick, Z. Anorg. Allg. Chem. **624**, 620 (1998).

[8] H. Lange, G. Wötting, and G. Winter, Angew. Chem., Int. Ed. Engl. **30**, 1579 (1991).

[9] M. Zeuner, S. Pagano, and W. Schnick, Angew. Chem., Int. Ed. **50**, (2011) (in press).

[10] A. Zerr, G. Miehe, G. Serghiou, M. Schwarz, E. Kroke, R. Riedel, H. Fuesz, P. Kroll, and R. Boehler, Nature (London) **400**, 340 (1999).

[11] K. Köllisch and W. Schnick, Angew. Chem., Int. Ed. Engl. **38**, 357 (1999).

[12] S.-D. Mo, L. Ouyang, W. Y. Ching, I. Tanaka, Y. Koyama, and R. Riedel, Phys. Rev. Lett. **83**, 5046 (1999).

[13] A. Zerr, R. Riedel, T. Sekine, J. E. Lowther, W. Y. Ching, and I. Tanaka, Adv. Mater. **18**, 2933 (2006).

[14] E. Soignard, D. Machon, P. F. McMillan, J. Dong, B. Xu, and K. Leinenweber, Chem. Mater. **17**, 5465 (2005).

[15] K. Leinenweber, M. O'Keeffe, M. Somayazulu, H. Hubert, P. F. McMillan, and G. H. Wolf, Chem. Eur. J. **5**, 3076 (1999).

[16] W. Y. Ching, Y.-N. Xu, and P. Rulis, Appl. Phys. Lett. **80**, 2904 (2002).

[17] P. Kroll and W. Schnick, Chem. Eur. J. **8**, 3530 (2002).

[18] K. Landskron, H. Huppertz, J. Senker, and W. Schnick, Angew. Chem., Int. Ed. **40**, 2643 (2001).

[19] G. Kresse and J. Hafner, Phys. Rev. B **47**, 558 (1993).

[20] G. Kresse and J. Furthmüller, Comput. Mater. Sci. **6**, 15 (1996).

[21] G. Kresse and J. Furthmüller, Phys. Rev. B **54**, 11169 (1996).

[22] W. Y. Ching, J. Am. Ceram. Soc. **73**, 3135 (1990).

[23] W. Y. Ching, J. Am. Ceram. Soc. **87**, 1996 (2004).

[24] W. Y. Ching, L. Ouyang, H. Yao, and Y. N. Xu, Phys. Rev. B **70**, 085105 (2004).

[25] Y.-N. Xu, P. Rulis, and W. Y. Ching, Phys. Rev. B **72**, 113101 (2005).

[26] A. Hussain, S. Aryal, P. Rulis, M. A. Choudhry, and W. Y. Ching, Phys. Rev. B **78**, 195102 (2008).

[27] L. Liang, P. Rulis, and W. Y. Ching, Acta Biomaterialia **6**, 3763 (2010).

[28] L. Liang, P. Rulis, B. Kahr, and W. Y. Ching, Phys. Rev. B **80**, 235132 (2009).

[29] L. Ouyang and W. Y. Ching, J. Appl. Phys. **95**, 7918 (2004).

[30] L. Ouyang, L. Randaccio, P. Rulis, E. Z. Kurmaev, A. Moewes, and W. Y. Ching, J. Mol. Struct. THEOCHEM **622**, 221 (2003).

[31] P. Rulis, W. Y. Ching, and M. Kohyama, Acta Mater. **52**, 3009 (2004).

[32] J. Chen, L. Ouyang, and W. Y. Ching, Acta Mater. **53**, 4111 (2005).

[33] P. Rulis, H. Yao, L. Ouyang, and W. Y. Ching, Phys. Rev. B **76**, 245410 (2007).

[34] W. Y. Ching, P. Rulis, L. Ouyang, S. Aryal, and A. Misra, Phys. Rev. B **81**, 214120 (2010).

[35] R. Dovesi, R. Orlando, B. Civalleri, C. Roetti, V. R. Saunders, and C. M. Zicovich-Wilson, Z. Kristallogr. **220**, 571 (2005).

[36] B. Delley, J. M. Seminario, and P. Politzer, in *Theoretical and Computational Chemistry* (Elsevier, New York, 1995), Vol. 2, p. 221.

[37] R. S. Mulliken, J. Chem. Phys. **23**, 1833 (1955).

[38] G. Onida, L. Reining, and A. Rubio, Rev. Mod. Phys. **74**, 601 (2002).

[39] R. F. Egarton, *Electron Energy-Loss Spectroscopy in the Electron Microscope* (Plenum, New York, 1996).

[40] S.-D. Mo and W. Y. Ching, Phys. Rev. B **62**, 7901 (2000).

[41] W.-Y. Ching and P. Rulis, J. Phys. Condens. Matter **21**, 104202 (2009).

[42] I. Tanaka, T. Mizoguchi, T. Sekine, H. He, K. Kimoto, T. Kobayashi, S.-D. Mo, and W. Y. Ching, Appl. Phys. Lett. **78**, 2134 (2001).

[43] W.-Y. Ching, S.-D. Mo, and Y. Chen, J. Am. Ceram. Soc. **85**, 11 (2002).

[44] T. Mizoguchi, I. Tanaka, S. Yoshioka, M. Kunisu, T. Yamamoto, and W. Y. Ching, Phys. Rev. B **70**, 045103 (2004).

[45] I. Tanaka *et al.*, Nat. Mater. **2**, 541 (2003).

[46] W. Y. Ching, L. Ouyang, P. Rulis, and I. Tanaka, Phys. Status Solidi B **242**, R94 (2005).

[47] T. Mizoguchi, A. Seko, M. Yoshiya, H. Yoshida, T. Yoshida, W. Y. Ching, and I. Tanaka, Phys. Rev. B **76**, 195125 (2007).

[48] W. Y. Ching and P. Rulis, Phys. Rev. B **77**, 035125 (2008).

[49] P. Rulis, L. Wang, and W. Y. Ching, Phys. Status Solidi RRL **3**, 133 (2009).

[50] P. Rulis, A. R. Lupini, S. J. Pennycook, and W. Y. Ching, Ultramicroscopy **109**, 1472 (2009).

[51] A. Altay, C. B. Carter, P. Rulis, W. Y. Ching, I. Arslan, and M. A. Gülgün, J. Solid State Chem. **183**, 1776 (2010).

[52] O. H. Nielsen and R. M. Martin, Phys. Rev. Lett. **50**, 697 (1983).

[53] R. Hill, Proc. Phys. Soc. A **65**, 349 (1952).

[54] H. Yao, L. Ouyang, and W.-Y. Ching, J. Am. Ceram. Soc. **90**, 3194 (2007).

[55] W. Y. Ching, L. Ouyang, P. Rulis, and H. Yao, Phys. Rev. B **78**, 014106 (2008).